Research Article Vol. 11, No. 8 / 1 August 2020 / Biomedical Optics Express 4679

Biomedical Optics EXPRESS

Optimizing infrared spectral discrimination to enhance disease diagnostics: monitoring the signatures of inflammatory bowel diseases with anti-TNFα therapy

HEMENDRA GHIMIRE,[1,4] XINJIE HU,[2] GENGSHENG QIN,[2,3] AND A. G. UNIL PERERA[1,3,4,*]

[1] Department of Physics and Astronomy, Georgia State University, Atlanta, GA 30303, USA
[2] Department of Mathematics and Statistics, Georgia State University, Atlanta, GA 30303, USA
[3] Center of Diagnostics and Therapeutics, Georgia State University, Atlanta, GA 30302, USA
[4] Interactions of radiation with matter laboratories, Georgia State University, Atlanta, GA 30303, USA
[*] uperera@gsu.edu

Abstract: This study presents an application of infrared spectroscopy of sera for monitoring the efficacy of anti-TNFα therapy for inflammatory bowel diseases. Understanding the therapeutic response includes the analysis of absorption bands representing constituent molecules. Interleukin-10 knockout mouse model of the diseases with anti-TNFα treatment was used. The discrimination potential is optimized by analyzing data with curve fitting. It shows; antibody therapy markedly ameliorated the disease, concurring with earlier mucosal immunology and pathophysiologic studies. This technique may thus also be useful for the evaluation of mucosal healing or other therapeutic modalities of gastrointestinal tract diseases keeping the endoscopic tests as confirmatory.

© 2020 Optical Society of America under the terms of the OSA Open Access Publishing Agreement

1. Introduction

Inflammatory bowel diseases (IBD), ulcerative colitis (UC) and Crohn's disease (CD) are debilitating with a chronically inflamed gastrointestinal (GI) tract [1]. It can limit an active lifestyle and lead towards the life-threatening complications [1], including secondary infections, organ degeneration, nutritional deficiencies, and even GI cancer [2]. Rapid detection and preventative interventions of these diseases enable the early administration of therapeutic strategies when the treatment is most effective. Simultaneous monitoring of mucosal healing during the treatment is also critical for IBD. Currently, endoscopic tests are commonly used to assess intestinal disease activities [3] including IBD. However, gold standard colonoscopy tests are expensive, invasive, risky, unpleasant for patients, and are not easily accessible to the eligible population for disease screening. It results in a decrease in the screening participation rates [4], despite strong recommendations. Endoscopic examinations are not also appropriate for frequent use while assessing treatment response and while predicting long-term outcomes [5].

The use of non- (or minimally) invasive stool or blood-based tests could increase the screening options and the patient's willingness for IBD screening participation. Studies [6,7] using attenuated total reflection Fourier transform infrared (ATR-FTIR) spectroscopy of serum samples has shown that IBD conditions are manifested in the molecular composition of serum, which can be measured relatively painlessly and conveniently. Presumably, studies [8] have shown that this technique would increase the adherence rate for disease screening. However, the sensitivity of this technique for unveiling therapeutic response subjective to IBD is not yet fully understood. Therefore, it is essential to understand the feasibility of the ATR-FTIR technique to monitor treatment efficacy by using serum samples. The understanding at the molecular level of changes

#394895 https://doi.org/10.1364/BOE.394895
Journal © 2020 Received 13 Apr 2020; revised 19 Jul 2020; accepted 20 Jul 2020; published 27 Jul 2020

Biomedical Optics EXPRESS

in diagnostic mediums as manifested in the infrared spectra will have great clinical significance to monitor disease progression or healing.

IBD patients tend to have a low interleukin 10 (IL10-/-) producer genotype (a regular cytokine that plays a major role in the homeostasis of the gut) more often than healthy controls [9,10]. Therefore, genetically engineered IL10-/- deficient mice were most frequently used as experimental models for chronic IBD studies. Longitudinal analysis of serum samples of IL10-/- mice using two-dimensional differential gel electrophoresis (2D-DIGE) proteomic analysis has shown that the accumulation of various proteins was altered under inflammatory conditions [11]. Importantly, a study has shown that this mouse model develops spontaneous chronic IBD and is showing a promise as a model for adequately recapitulate the full complexity of the human disease [11]. Appropriateness of IL10-/- mouse model to analyze the multifactorial nature of this disease including genetic factors, immune aspects and the role of the microbiota contributing to IBD is also reported [12]. Similarly, IBD patients tend to have an increased level of the tumor necrosis factor (TNF) in serum, stool, or mucosal biopsy specimens [13]. Tumor necrosis factor-alpha (TNFα) is a cell-signaling protein (cytokine) that plays a central role in inflammation. Therefore, TNFα became a key target for antibody treatment for inflammation [12]. It is found that the diversity of fecal microbiota in the IBD patients shifts towards the control individuals [14] after anti-TNF therapy. This treatment option leads to mucosal healing, reducing hospitalizations, and surgeries while improving patients' quality of life [15]. Experiments on IL10-/- deficient mouse models [16] also demonstrates the same outcomes [17]. The cytokines in the stool samples showed that the debilitating IBD conditions of IL10-/- deficient mice can be improved by anti-TNFα antibody therapy [18].

The study presented in this manuscript demonstrates ATR-FTIR spectroscopy of serum samples to analyze biochemical changes in samples of IBD mice and treated mice. IL10-/- mice treated with and without anti-TNFα antibody therapy were used to understand the efficacy of the technique for drug signature monitoring. As such, the present study is not only applicable to understand the molecular mechanism that promotes or lessens IBD but also to understand the feasibility of the technique in the clinical domain. An appropriate optical design offering better interaction of the incident photons with samples and extracts good spectra is presented. The optimization, instrumentation, including the integration feasibility of data analyzing software, is also discussed.

2. Materials and methods

The current study is a follow up to our previous study [7]. In our earlier studies [6,7], we found that infrared spectral signatures representing mannose and the protein secondary structures are unique to IBD differing from arthritis and metabolic syndrome models. The statistical measures of additional signatures and the potential clinical application of the technique are also discussed in this present study. A short description of animal models, sample preparation, and instrumentation were previously presented [7], but here we present the methodology in detail for optimization in measurement and data analysis techniques. Additionally, differing from our earlier study, we have improved the resolution from 8 cm^{-1} to 4 cm^{-1}, increased the identifying markers from two to six, and compare the diagnostic accuracy by using sensitivity, specificity, and AUC values. The snapshot of IBD-associated alteration in circulating carbohydrates and nucleic acids is also evaluated by extending the spectral fitting protocol to the complex region, 1140-1000 cm^{-1}. All studies were performed following the Institutional Animal Care and Use Committee at Georgia State University (Atlanta, GA), permit number: A14010.

2.1. Animal growth and sample preparation

The IL10-/- mouse model develops IBD in a time-dependent manner [16]. Similarly, the anti-TNFα treatment on IL10-/- mice shows the therapeutic efficacy in resolving intestinal

Biomedical Optics EXPRESS

inflammation [17]. A study indicates that IBD development and their healing is independent of sex (male or female) in IL10-/- mouse [18].

In this study, eighteen, three weeks-old female (IL10-/-) knockouts mice, obtained from Jackson Laboratories (Bar Harbor, ME), were used. Nine mice were treated with anti-TNFα therapy, twice a week by intraperitoneal injection of anti-TNF antibody, starting from the 28th day of their birth, and the remaining mice (n=9) are treated with Phosphate buffered saline (PBS). Feces collected on day 28 (4 weeks) and day 98 (14 weeks), and Lipocalin-2 (Lcn-2) was measured to assess the intestinal inflammation in those mice [19]. Total RNA was also extracted from colon tissues to analyze the effect of anti-TNF treatment.

Similarly, blood samples collected on day 28 and day 98 was centrifuged by using serum separator tubes for IR spectral measurements. Herein, samples collected from mice on day 28, before they develop colitis constitute the control or non-colitis (n=16). The samples extracted on days 98 of PBS injected mice are colitis (n=9). Similarly, the samples extracted on days 98 from anti- TNFα injected colitis- mice are treated (n=9).

2.2. Effect of anti-TNFα therapy

Anti-TNF drugs have proven highly effective for targeting and diminishing the downstream effects of TNFα activation. However, the precise mechanism is still unclear [20]. Studies have shown that a significant proportion of patients do not respond to the treatment, or they lose the effect over time. Therefore, 30-40% of CD patients and 25-30% of UC patients still need surgery at some point during their life addition to the biological treatment [21,22]. Herein, we have analyzed microRNAs (miRNAs) to analyze the efficacy of anti-TNF treatment. It is noted that miRNAs are promising biomarkers for IBD [23]. We examined the expression levels of pro-inflammatory cytokines in the colon, to understand the response of therapeutics. Herein, the colonic miRNA expression analysis is performed by the quantitative polymerase chain reaction (qPCR) by following the protocol as discussed [23].

2.3. Equipment setup

A Bruker; Vertex 70 FTIR spectrometer with KBr beam splitter, and deuterated triglycine sulfate (DTGS) detector was used. Medium Blackman-Harris apodization [24] at room temperature was used. Resolution of 4 cm^{-1} with a zero-filling factor of 4 is also employed to give a data spacing of 1 cm^{-1}. Herein, the resolution is improved from our earlier studies (where we used resolution 8 cm^{-1} [7]), and integration with strong apodization function [24] was implemented. The IR light beam intensity was controlled by passing it through a 2.5 mm aperture. A Parker-Ballston gas purging system was also used to maintain purified ambient air in the spectrometer. We have performed repeated measurements and extract information from several studies, including Refs. [25] and protocol [26] while selecting these parameters. This selection allows us to reduce noise, and to analyze the spectral data without losing information during spectral deconvolution. Resolution of 2 cm^{-1} gives noisy derivatives spectra and of 8 cm^{-1} resolution gives rise to missing secondary structures information (spectral markers show less degree of variability), while using diamond ATR crystal configured to have a single reflection of incident infrared radiation.

An ATR accessory from Harrick-Scientific with a diamond crystal (1 mm x 1.5 mm and is configured to have a single reflection of the incident radiation) was used as an internal reflection element of the IR radiation. The ATR sampling mode [26] is considered as ideal for strongly absorbing body fluids and offers a rapid and reliable way for clinical applications [25]. In this mode, light is reflected (Fig. 1(A)) inside the prism (ATR crystal) of the high refractive index [27], and the reflected light from the sample (Goos-Hanchen effect) [28] creates an evanescent wave, penetrating the sample placed in contact with crystal [29]. The penetration depth of

Biomedical Optics EXPRESS

evanescent waves is given by the equation, $d_p = \lambda/2\pi\left(n_1{}^2 Sin^2\theta - n_2{}^2\right)^{1/2}$ depending on the wavelength of the incident radiation (λ), the refractive index of the crystal (n_1), the angle of incidence (θ), and the refractive index of the sample (n_2). Diamond has a smaller acceptance angle cone, which allows having a good optical design to extract good spectra. Because of the strong robust, and chemically inert feature of the diamond, it is considered as the best ATR crystal for routine measurements of biological samples [30]. Thus, most optimized values of measurement parameters are used in this experimental and equipment setup.

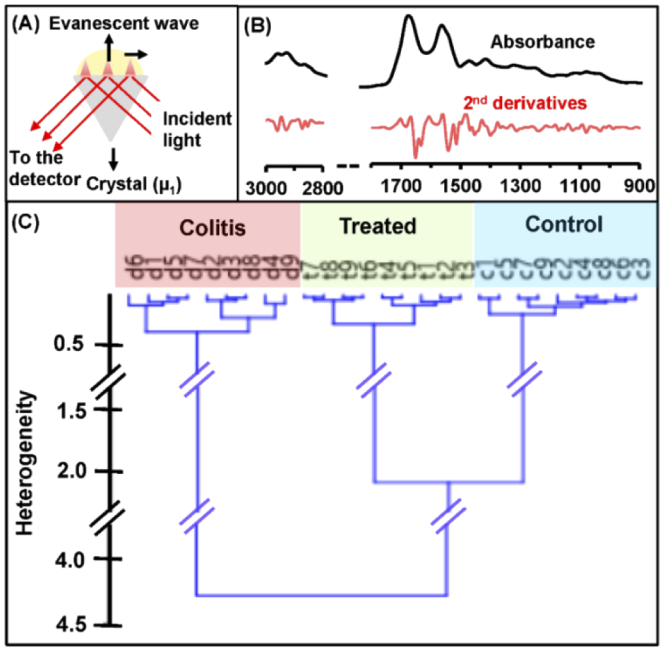

Fig. 1. (A) Light-sample interaction and formation of the evanescent wave, which extends into the sample in ATR sampling mode. The beam is then collected by a detector as it exits the crystal. (B) Absorbance spectra and its second derivative curve. The measurement was taken at a resolution of 4 cm^{-1}. (C) Dendrogram tree diagram performed, by using Ward's algorithm and Euclidian distance measurements of vector normalized second derivative curves within spectral range 1600-1700cm^{-1}. A wide difference can be seen between spectra belonging to control and colitis mouse, compared to the degree of the dissimilarity between controls and treated.

Figure 1(B) shows the absorbance spectra measured at a resolution of 4 cm^{-1} and its second derivatives curve. In infrared spectroscopy, derivatives analysis helps us to accentuate small differences (by reducing the replicate variability, correct baseline shift, resolve overlapping peaks, and simplify spectra variations) between two nearly identical spectra. It also assists us to determine the number of bands and their wavelengths and has been used in various spectral discrimination techniques [31]. In this study, we analyze the absorbance spectra and its second derivative curves.

2.4. Spectral measurement

The surface of ATR crystal was first cleaned with sterile phosphate-buffered saline (PBS) solution and by ethanol. The cleanliness test was then conducted to ensure there are no signal peaks higher than the environmental noise level. Background measurement, showing the presence of any environmental residue on the crystal surface or in the light path, was performed on a clean

Biomedical Optics EXPRESS

surface before each measurement. It allows us to get high-quality spectra using background corrections. Serum samples (1 μL) are deposited on the crystal surface and allowed to air dry (~8 minutes) at room temperature. An evanescent wave produced at the interface by the internal reflection of light interacts with the layer of the sample within the penetration depth [32]. Each sample was scanned multiple times to get ten or more high-quality (exactly overlapping) spectral data within the mid-infrared range 400 to 4000 cm^{-1} and 6 reads of the 100 co-added scans for each sample (total of 600 scans) were averaged. Using OPUS 6.5 software, all the spectra were min-max normalized by scaling the range 1800 to 900 cm^{-1}. This range comprises a significant biochemical fingerprint of the biological material and the amides (I and II) bands [26]. Vector normalization [33] is another popular protocol where the average absorbance is subtracted from each data point, and the spectrum is divided by the square root of the sum of squares of absorbance. In general, the normalization protocol [26] can be chosen to best serve the purpose of comparison. In this study, min-max normalization to the amide I peak is employed as it emphasizes the deviation between the colitis and control sample spectra. Min-max normalized absorbance spectra were then sectioned within the range of 1800 to 900 cm^{-1} for further analysis. We have also performed vector normalization of second derivatives spectra while comparing them.

2.5. Spectral analysis

Our analysis includes the dendrogram of hierarchical cluster analysis (HCA), which is commonly employed to identify the similarities between the FTIR spectra by using the distances between frequencies and aggregation algorithms [34]. Using the "PAST (PAleontological STatistics [35]) 4 - the Past of the Future" software and the vector normalized second derivative curve of the absorbance spectra within 1600-1700 cm^{-1} as input data (variables), HCA is performed and the dendrogram is plotted. Dendrogram tree diagram performed, using Ward's algorithm and Euclidian distance measurements, allow us to visualize the overall classification as shown in Fig. 1(C). In both analyses, spectral data from an equal number of mice were used (herein, we have randomly picked 9 controls). However, the degree of heterogeneity is less for treated groups from control group compared with colitis. Herein, HCA analysis allows us to understand the preliminary idea about the potential application of the measurement techniques to segregate the groups.

In order to optimize the discrimination, we perform quantitative analysis of absorption band values at different biomarkers positions, which follows discrimination of secondary structures by deconvolution of the spectra in the amide I region. During the deconvolution process, the computed curve that best fit with the experimental spectrum is obtained from the superposition of Gaussian function energy bands (GFEB). The individual Gaussian bands from deconvolution represent proteins' secondary structures as discussed in the similar studies in the field [36–41] used to verify the applicability of this technique over complementary spectroscopic methods (X-ray crystallography, and nuclear magnetic resonance).

The process of deconvolution includes sectioning of min-max normalized spectra followed by rubber-band correction with two baseline points, such that absorbance values at two ends of the selected region will be zero. These spectra were then fitted with GFEBs by approximating the position and the number of bands from the minima of second derivative spectra (Fig. 2(A)) and also by the minimization of root mean square (RMS) error via the Levenberg-Marquardt [42] algorithm. In the fitting process position, height, width, and hence integral values are varied such that the simulated curve best fits the experimental curve [43,44]. Herein, the goodness of the fit is determined by the convergence of the RMS error or the residual to a singular minimum value. Figure 2(B) shows the spectral fitting within amide I. Using six bands with corresponding biological components; side chain, beta-sheet, alpha helix, disordered structure, and beta turns, we found that fitting solution is unique as determined by the second derivative. The minima

Biomedical Optics EXPRESS

(position and number) of the second derivatives of the spectral curves reflect the positions and the number of bands needed to fit the spectral curve. The minor variation of the positions of the six bands are all within the acceptable ranges [45] for those biological components. Similarly, by choosing the number and positions of bands indicated, excellent RMS error values are obtained, between 0.0034 and 0.0035 for all 34 studies. It further allows us to overcome the challenges [46] of deconvolution process for quantitative analysis. Herein, by normalizing and sub-sectioning, the amide-I region of absorption spectra followed by baseline correction and spectral fitting, the effects of the bands describing individual biological components allow us for a more precise analysis of the spectra, thereby increasing confidence while comparing two states.

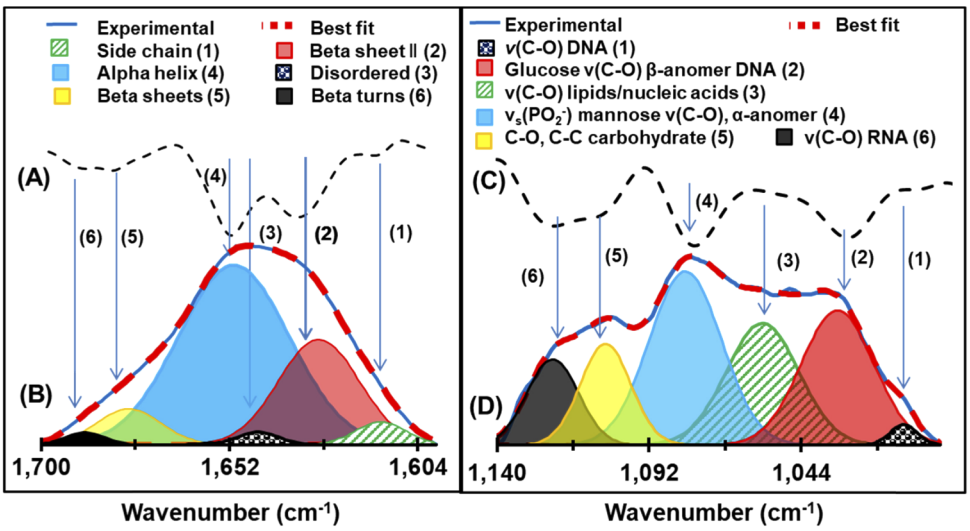

Fig. 2. The process of spectral deconvolution. (A) Second derivative spectra of amide I absorbance curve 1600-1700cm^{-1}. (B) Gaussian function energy bands used to obtain a curve that fits the experimental absorption curve. (C) Second derivative spectra of nucleic acids and carbohydrates complex band 1000-1140 cm^{-1}. (D) Deconvolution of the complex band by estimating number and position using minima of second derivatives curve.

Similarly, the complex region [47] of carbohydrates and nucleic acids 1140-1000 cm^{-1} is deconvoluted with six GFEB, describing individual biological components is as shown in Fig. 2(D). The number and positions of GFEBs are again approximated by using the minima of second derivatives (Fig. 2(C)). The sum of the integral areas covered by six bands was further statistically analyzed.

2.6. Statistical measures

Quantified values of these identifying spectral signatures are statistically analyzed to see the colitis-associated alteration in the blood serum, and their stabilization after biological therapy. Our statistical analysis mainly includes finding the sensitivity and specificity of the markers for their discrimination. Sensitivity and Specificity of a diagnostic test are often used to describe the diagnostic accuracy/performance of the analysis in biomedical research [48]. The discriminating potential of a diagnostic regimen can be quantified by the Youden index and the area under the receiver operating characteristic (ROC) curves [49]. The ROC curve is plotted to find the area under the curve (AUC). The optimal cutoff value calculated based on the Youden index for each spectral marker is used to select the positivity/negativity of the disease and to estimate the sensitivity and specificity.

Biomedical Optics EXPRESS

3. Result and discussion

3.1. Comparing normalized absorbance

To monitor the therapeutic response of colitis, we examine the chemical composition of serum samples derived from non-colitis, colitis and anti-TNFα treated IL10-/- mice. Figure 3(A) shows average representations of the normalized absorption spectra of serum samples derived from each mice type. Herein, we have monitored previously identified IR spectral signatures [6–8] for colitis in diseased species with anti-TNFα antibody therapy, which displays exciting results. The alteration in the IR absorption values due to colitis in IL10-/- mice come close to control mice in anti-TNFα treatment treated cases.

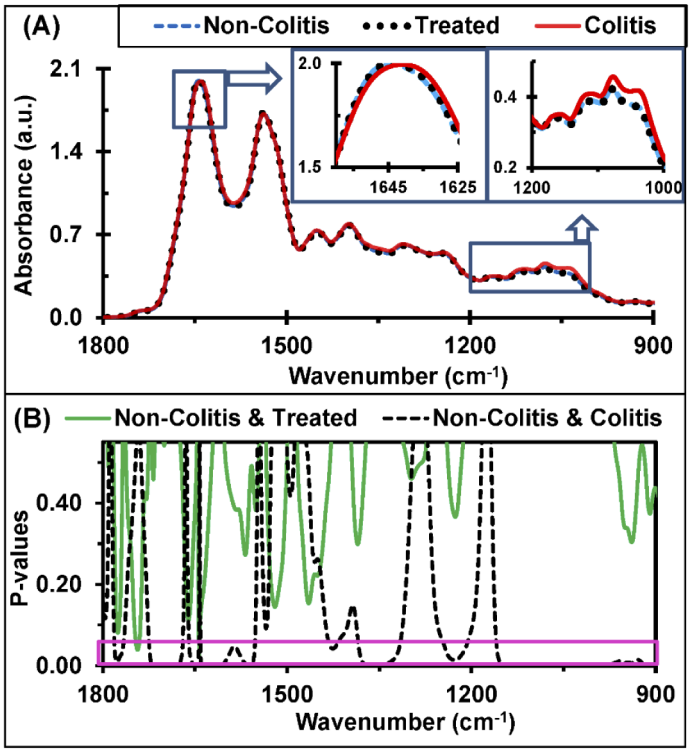

Fig. 3. Normalized absorbance and p-value calculation. (A) Averaged ATR-FTIR spectra of serum samples, derived from control (Non-Colitis, n=16), treated with anti-TNFα antibody (Treated, n=9) and colitis untreated (Colitis, n=9) mice. These spectra show proper anti-TNFα therapy ameliorate the colitis disease. Inset shows magnification within 1200-1000 cm^{-1} and 1660-1625 cm^{-1}, which clearly shows how the absorbance curve of anti-TNFα treatment comes close to the control levels. (B) P-value calculation of colitis and treated conditions with control types. P-value is less than 0.05 at various spectral bands while comparing non-colitis and colitis, but it is always greater than 0.05 while comparing non-colitis and treated. The region highlighted by the pink box (□) is the region with $p \leq 0.05$.

The student t-test p-values on absorption spectra representing normal, colitis, and antibody-treated colitis mice are as given in Fig. 3(B). It shows how absorption values vary with control with treated and the control with colitis within the entire wavelength region 900-1800 cm^{-1}. Throughout the whole wavelength region, the differentiating signatures better than 95% (or higher) are highlighted by the shadowed area. Herein, the spectral regions with p-values less

Biomedical Optics EXPRESS

than 0.05 are selected as having significant variations between the non-colitis and colitis. The assignment of these spectral regions/bands include; 1766-1780 cm^{-1} (C = O of lipids), 1670-1710 cm^{-1} (amide I of proteins), 1548-1649 cm^{-1} (amide I and amide II of proteins), 1317-1383 cm^{-1} (CH_3/CH_2 bending), 1208-1244 cm^{-1} (asymmetric PO_2 stretching of phosphate lipids), and 900-1159 cm^{-1} (the mixed region of carbohydrates, and nucleic acids). Due to the complexity of biological systems, biomolecular and bonding vibration assignments are tentative and are based on numerous studies [50–58]. The biomolecular assignments of the discriminatory spectral bands and their bond vibrations are shown in Table 1. The colitis associated changes in all these spectral bands come to the level of control in anti-TNF α antibody therapy mouse serum.

Table 1. Discriminatory infrared spectral bands, with assignments and their bond vibrations.

Band (cm^{-1})	Assignment and vibrations [50–58]
900-1158	Carbohydrates [51,52] (Glucose, Mannose, Fructose) and nucleic acids (Deoxyribose/Ribose DNA, RNA) [50]: C-O, C-C stretch, C-H bends, Endocyclic C-O-C vibration and, νs(PO^{2-}) [54]
1208-1244	Amide III, νas(PO^{2-}) [55]
1317-1382	Collagen: CH_2 wagging, the vibration of α, and β anamor [56].
1420-1430	Polysaccharides, νs (COO^-), δ(CH_2)
1480-1580	Amide II of proteins: (α-helical, β-pleated sheet, unordered conformation structures), δ(N-H), ν(C-N) [58].
1600-1700	Amide I of proteins: (α-helical, β-pleated sheet, β-turns, random coils, and side-chain, β (anti-‖+turn) structures), ν(C = O), ν(C-N), CNN [58].
1720-1750	Lipids C = O stretching [57]

3.2. Identifying discriminatory spectral bands

Identifying spectral signatures in this study include: (a) absorption values at wavenumber 1033 cm^{-1} (I_{1033}), primarily due to glucose [6] presence; (b) absorption values at wavenumber 1076 cm^{-1} (I_{1076}), representing the mannose [6] as well as phosphate presence; (c) the ratio of absorbance at wavenumber 1121 cm^{-1}, associated with RNA presence, to its value at 1020 cm^{-1}, associated with DNA presence [47] (I_{1121}/I_{1020}); (d) the ratio of absorbance at wavenumber 1629 cm^{-1}, indicating the protein presence, to 1737 cm^{-1} signaling the presence of lipids (I_{1629}/I_{1737}); (e) the ratio of Gaussian function energy bands representing α helix and β sheet protein secondary structures as obtained from the deconvolution of amide I region; and (f) the sum of the integral area of GFEBs used to fit the experimental curve within the complex band of carbohydrates, and nucleic acids 1000-1140 cm^{-1}. Earlier, various serological markers were analyzed for IBD diagnosis [59] and discrimination of IBD types [60]. These studies have reported abnormalities in lipids, amino acids, and energy metabolisms in the serum samples of IBD patients [61]. Associations between fatty acids and inflammatory cytokines or the protein abundance and the epigenetic alteration in the samples of IBD patients have been also established [62]. Similarly, proteomic analysis in serum samples of IL10-/- mice shows alterations of various proteins [11] under inflammatory conditions. The protein secondary structure alterations could be due to a melded manifestation of these protein variations. As such, variations in these reported serological markers are most likely the primary reason for the IBD induced changes in absorption frequencies of functional groups of proteins, carbohydrates, nucleic acids, and lipids.

The representation of ensemble averages for identifying five spectral markers, I_{1033}, I_{1076}, I_{1121}/I_{1020}, I_{1629}/I_{1737}, integral ratio (α/β), and the sum of the area of GFEBs used to fit 1000-1140 cm^{-1} are shown in Fig. 4. Absorption values representing the glucose peak position at 1033 cm^{-1} is shown in Fig. 4(A), and this value at the mannose peak position 1076 cm^{-1} is shown in Fig. 4(B). The average ratio of the RNA peak to DNA peak (I_{1121}/I_{1020}) is as indicated in

Biomedical Optics EXPRESS

Fig. 4(C), and the average ratio of the peak representing protein to lipid peak is shown in Fig. 4(D). Figure 4(E) and Fig. 4(F) shows the integral values of the α-helix and β-sheet protein secondary structures, respectively. Similarly, the average integral ratio of α-helix to the β-sheet structure is shown in Fig. 4(G). The sum of integral values of Gaussian bands used to fit the experimental curve within 1000-1140 cm^{-1} are shown in Fig. 4(H). These absorption and ratio values are also tabulated in Table 2.

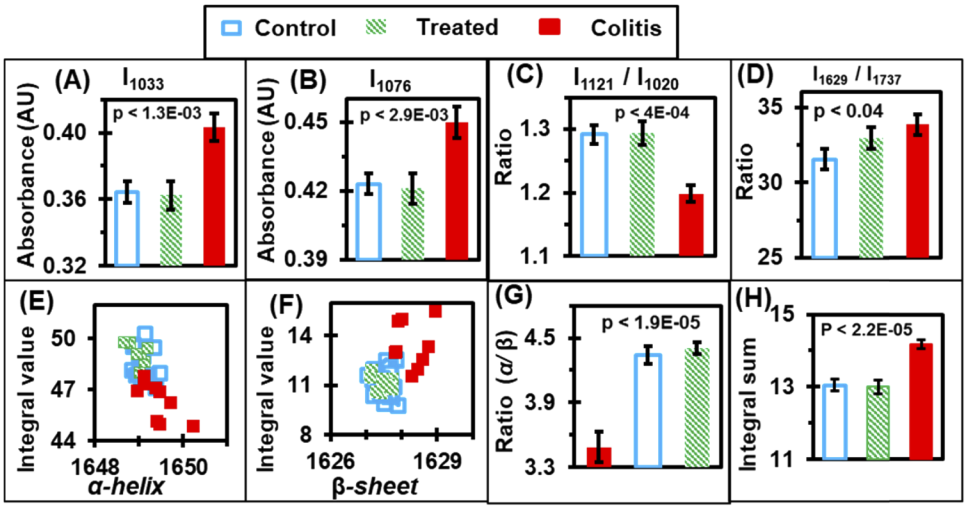

Fig. 4. Representation of identifying spectral markers. (A) Ensemble average representative of absorbance of wavenumber position 1033 cm^{-1}. (B) Ensemble average representative of absorbance of wavenumber position 1076 cm^{-1}. (C) The ratio of absorption values at wavenumber 1121 cm^{-1} to 1020 cm^{-1}. (D) The ratio of absorbance at wavenumber 1629 cm^{-1} to 1737cm^{-1}. (E) The integral values of Gaussian function energy bands representing the α helical structure of protein secondary structure. (F) The integral values of Gaussian function energy bands representing the β pleated sheet structure of protein secondary structure. (G) The integral ratio of α-helix and β-sheet protein secondary structures. It shows the level of β sheet structure increase and α helix drops due to colitis and their resettlement in anti- TNF α therapy mice. (H) The sum of the integral area of GFEBs used to fit the experimental curve in the complex band 1000-1140 cm^{-1}.

Table 2. Quantified values of identified spectral markers: I1033, I1076, I1121/I1020, I1629/I1737, integral ratio (α/β), and the sum of the integral area of GFEBs used to fit the experimental complex band 1000-1140 cm-1. Tabulated p-values represent a comparison between control and colitis.

Markers Specifications	Glucose (1033 cm^{-1})	Mannose (1076 cm^{-1})	RNA/DNA (1121/1020)	Protein/Lipid (1629/1737)	Integral Ratio (α/β)	Integral sum Complex band
Control	0.36 ± 0.01	0.42 ± 0.01	1.29 ± 0.02	31.54 ± 0.69	4.34 ± 0.09	13.04 ± 0.16
Colitis	0.41 ± 0.01	0.46 ± 0.01	1.19 ± 0.01	33.85 ± 0.69	4.40 ± 0.06	14.17 ± 0.12
Treated	0.36 ± 0.01	0.42 ± 0.01	1.29 ± 0.02	32.98 ± 0.73	3.49 ± 0.14	13.0 ± 0.18
P-value	1.3E-03	2.9E-03	4E-04	0.04	1.9E-05	2.1E-05

Although, the precise mechanism of anti-TNFα treatment in IL10-/- mice is still unknown [20], our experimental demonstration verifies the efficacy of infrared spectroscopy to monitor disease associated changes in serum constituents. Our study also verifies the efficacy of anti-TNFα treatments to restore these altered constituents to the level of control. The quantitative analysis

Biomedical Optics EXPRESS

of signatures; I_{1033}, I_{1076}, I_{1121}/I_{1020}, I_{1629}/I_{1737}, integral ratio (α/β), and the sum of the area of GFEBs used to fit 1000-1140 cm^{-1} comes close to each other for the controls and the anti-TNFα treated cases indicating no significant statistical difference between the two sets. Since the focus of this work is to identify the infrared signatures, regaining (or restoring) of altered spectral markers of IBD close to the control level in anti-TNFα treatment is an important finding.

3.3. Statistical analysis

The heterogeneity between each study type is further tested by using quantitative analysis that involves the calculation of Youden's index, the area under the receiver operating characteristic (ROC) curves, sensitivity, specificity, and the calculated p-value [49]. Statistical measures [48] of these discrimination techniques also reveal the feasibility of the studied monitoring regimen in the clinical domain. The ROC curves are plotted to find the area under the curve (AUC); for each of these features, the threshold values were used to estimate the sensitivity and specificity. Then, the Youden index, (the maximum of sensitivity + specificity – 1), was used to find the optimal cutoff values among the threshold values. Herein, Fig. 5(A) shows the confirmation of the effect of anti-TNFα therapy in studying mouse groups evaluated by analyzing expression levels of TNFα in the total RNAs extracted from colons. ROC plots for the (α/β) signature are shown in Fig. 5(B). The maximum sensitivity and specificity of this particular signature were found to be 100% and 81%, respectively. Sensitivity and specificity are major concerns in such studies and analysis led to the identification of statistically significant differences in IR spectral markers between non-colitis, IL10-/- induced colitis, and with anti-TNFα treated mice experiments. Sensitivity, specificity, and AUC values are calculated for all the identifying spectral signatures as shown in Table 3. Statistically, significant differences can be seen between non-colitis and colitis conditions for identifying signatures. However, while comparing control and the treated conditions, approximately 50% (0.5) AUC values can be obtained showing there is no class separation. AUC values while comparing control and treated are 0.54, 0.56, 0.49, 0.66, 0.46 and 0.55 for the spectral signatures: I_{1033}, I_{1076}, I_{1121}/I_{1020}, I_{1629}/I_{1737}, integral ratio (α/β), and the integral sum, respectively. Since the AUC values of colitis and non-colitis are higher (close to 90%) and that of non-colitis and treated is close to 50%, showing these spectral signatures can be applicable for drug signature monitoring. Having shown the discriminating potential of the present diagnostic regimen; it is essential to study many samples producing acceptable sensitivity and specificity values. Discriminating temporal variation during disease progression or its suppression is also a critical follow-up step.

Table 3. Sensitivity, specificity and AUC value calculations of identifying spectral markers.

Specifications	Markers					
	Glucose (1033 cm^{-1})	Mannose (1076 cm^{-1})	RNA/DNA (1121/1020)	Protein/Lipid (1629/1737)	Integral Ratio (α/β)	Integral sum Complex band
Sensitivity	89	89	100	90	100	100
Specificity	88	88	75	56	81	75
AUC	0.88	0.86	0.90	0.73	0.95	0.92

The present study provides a detailed insight into the molecular structural changes in serum samples of the IL10-/- IBD mouse model. Infrared spectral signatures representing proteins, carbohydrates, nucleic acids, and lipids are identified as the potential markers reflecting molecular changes. The success of the present technique in measuring the effect of anti-TNFα on the identified spectral signatures will provide an additional level of information about the treatment option of IBD patients and will increase the possibility of adapting this technique for disease status monitoring. Addressing the cost and hassle of colonoscopy that discourages people from being

Biomedical Optics EXPRESS

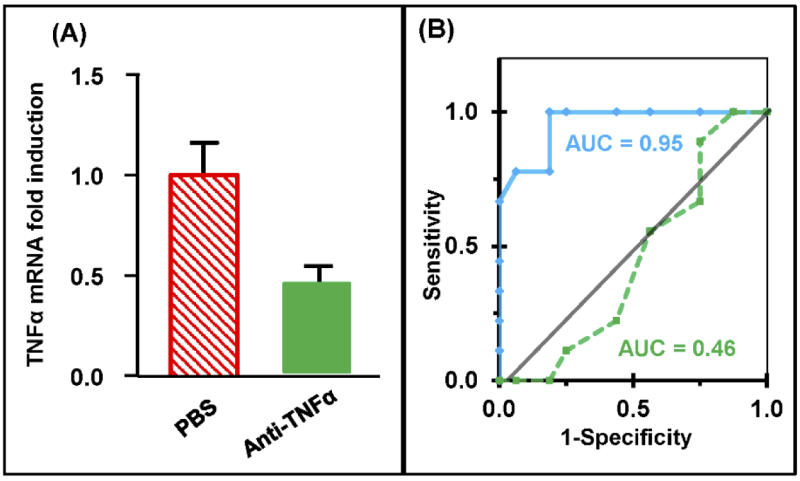

Fig. 5. (A) The expression levels of TNFα in the Total RNAs extracted from colons. The level of TNFα is quantified by qPCR and it confirms the effect of anti-TNFα therapy. (B) ROC curve for the data obtained from the ratio of the integral area of energy bands representing α-helix and β-sheet protein secondary structures. AUC is 0.95 while comparing colitis and non-colitis, but its value is 0.46 while comparing non-colitis and the treated. High diagnostic accuracy (with AUC = 0.95) can be seen for colitis, but poor diagnostic accuracy (with AUC = 0.46) for the treated.

screened timely, doctors, particularly primary care physicians can make their patients more aware of infrared spectroscopic analysis of blood serum. If the test shows an indication of diseases, colonoscopy can be performed. However, at its present form, the molecular mapping in serum samples as the infrared signatures of the disease cannot replace gold standard colonoscopy tests, but will provide additional information about the IBD patients before colonoscopy. Therefore, the feasibility of FTIR spectroscopy to extract a snapshot of cumulative molecular interactions within mouse serum samples for IBD study warrant a thorough investigation, as enabled by interdisciplinary collaboration between spectroscopists, biologists, and clinicians.

Using a statistically significant number of experimental mouse models with different stages of disease progression and healing can establish an association between identifying spectral marker changes with the disease stage. Mouse model study helps us to establish an association between spectral signatures of IBDs with histological findings of intestinal tissues. Understanding the association between identifying spectral signatures and the abolition or restoration of tissue functions in the intestinal tract is important because lymphocytes infiltrations and erosion of crypt can be seen in the diseased IL10-/- mice [6]. Additionally, by building a logistic regression model for the spectral features and doing cross-validation, a correlation between the degree of variation in spectral markers and the level of Lcn-2 in their stool or myeloperoxidase (MPO) activity of the distal colon [6] can be established. Research into samples of mice with intermediate stages of the disease will provide more insights into the evolution of healing and add confidence to the analysis and the applicability of the technique for early diagnostics. However, the animal models are not enough for preclinical human disease studies and for confirming the potential clinical effects in humans. Therefore, a follow-up step would be to analyze a statistically significant number of human samples to examine covariate effects of demographic and clinicopathological variables like age, weight, ethnicity, diet, disease stage, and comorbidities on the spectral signatures.

Biomedical Optics EXPRESS

4. Conclusion

The application of ATR-FTIR spectroscopy to identify treatment effects of anti-TNFα in IL-10-/- genotype IBD mouse model is demonstrated. By measuring spectra of serum samples of Colitis, anti- TNFα treated and Non-colitis mice, we have compared the statistical significance difference between the groups and identify the discriminatory features. Identifying infrared spectral signatures I_{1033}, I_{1076}, I_{1121}/I_{1020}, I_{1629}/I_{1737}, α-helix/β-sheet, and integral sum verify antibody therapy markedly ameliorated the disease as judged by earlier studies [15]. These data justify more initial findings [6–8] and support the feasibility of this regimen for drug management during its treatment. The study of ATR-FTIR spectroscopy of serum samples thus needs to extend with a statistically significant number of experimental models and human participants.

Importantly, the standardization of technique for the acquisition of spectral signatures applicable in the clinical domain is explored. The improved standardization of spectral signature acquisition is needed to assure the potential clinical application of the technique for IBD screening. The standardization includes reducing the unwanted experimental and data analysis specific variances. Herein, using a trial-and-error based approach and the clinically relevant data sets on ATR-FTIR spectroscopy of serum samples, most optimized parameters were used throughout the study. Diagnostic performance parameters, such as sensitivity, specificity, and AUC under ROC curves prove the feasibility of the studied technique.

Furthermore, the fully automated, user-friendly tabletop screening technique integrated with measurement and data handling approaches can be developed. Similarly, by using quantified spectral signatures, a software program that can be controlled by technicians in the clinical domain can also be developed. Identifying infrared signatures of disease allow us to create user-friendly instrumentation, integrated with intelligent software packages for presenting the diagnostic/screening potential, feasible for clinicians. Schematic of potential user-friendly, ATR-FTIR spectroscopy unit integrated with automated data analysis software (as indicated in our earlier study [8]) is shown in Fig. 6. Instrument control (μ-controller (I)) and data management software (μ-controller (II)) allow us to acquire spectral data and process them. The software package in the controller (II) includes data record, averaging, normalization, deconvolution, followed by the quantification. The integration of such intelligent software packages with the advanced portable FTIR spectroscopy allows technicians' a complex process to be simplified to deposit the sample and obtain the diagnostic decision with a single mouse click.

All in all, the available screening/diagnostic techniques for IBD, such as colonoscopy, sigmoidoscopy, and small bowel follow-through [63], have high sensitivity. Nonetheless, these techniques are invasive and expensive due to the need for specialized instruments and qualified personnel, require prior preparation and cause discomfort with associated risks of colonic perforation, hemorrhaging post-polypectomy electrocoagulation syndrome and infections. The present study provides evidence that ATR-FTIR spectroscopy of serum samples accompanied by data analysis techniques could be a tool to evaluate anti-TNFα therapy in IBD. The study also provides a detailed insight into the techniques and instrumentation for its clinical applications. The understanding the drug signature efficacy by using IR spectroscopy of serum samples strengthening the idea of the potential applicability of the technique. It is because; the access to this screening technique would increase the likelihood of compliance with screening recommendations for those who are otherwise reluctant to undergo the existing endoscopic tests.

Biomedical Optics EXPRESS

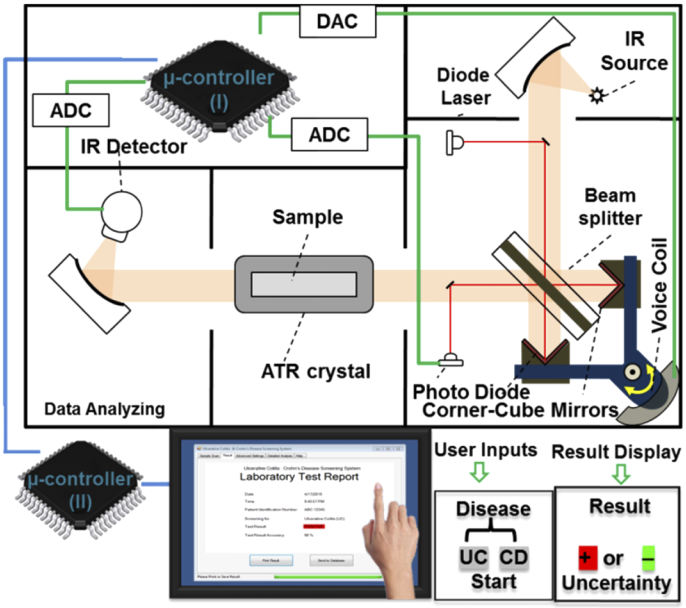

Fig. 6. Schematic of ATR-FTIR spectroscopy integrated with data analysis facility. Micro (μ)-controller (I) controls all the functions within the FTIR instruments, while μ-controller (II) takes care of the spectral response analysis.

Funding

Army Research Office (W911 NF-15-1-0018).

Acknowledgments

We are thankful to Dr. Emilie Viennois and Dr. Didier Merlin at the institute for biomedical sciences, GSU, Atlanta, GA 30302, USA. The serum samples and the guidance they provided throughout are much appreciated. We also want to acknowledge P. V. V. Jayaweera at SPD Laboratory, Inc., Hamamatsu, Japan, for his idea to develop the possibility of μ-controllers applicable in portable device development. H. Ghimire wants to acknowledge MBD program and the dissertation (internal) grant program at GSU for their support.

Disclosures

"The authors declare no conflicts of interest."

References

1. D. N. Frank, A. L. S. Amand, R. A. Feldman, E. C. Boedeker, N. Harpaz, and N. R. Pace, "Molecular-phylogenetic characterization of microbial community imbalances in human inflammatory bowel diseases," Proc. Natl. Acad. Sci. **104**(34), 13780–13785 (2007).
2. S. H. Itzkowitz and X. Yio, "Inflammation and cancer IV. Colorectal cancer in inflammatory bowel disease: the role of inflammation," Am. J. Physiol. Gastrointest. Liver Physiol. **287**(1), G7–G17 (2004).
3. D. W. Hommes and S. J. J. G. van Deventer, "Endoscopy in inflammatory bowel diseases," Gastroenterology **126**(6), 1561–1573 (2004).
4. A. R. Green, A. Peters-Lewis, S. Percac-Lima, J. R. Betancourt, J. M. Richter, M.-P. R. Janairo, G. Gamba, and S. A. Atlas, "Barriers to screening colonoscopy for low-income Latino and white patients in an urban community health center," J. Gen. Intern. Med. **23**(6), 834–840 (2008).
5. M. Dave and E. V. Loftus Jr, "Mucosal healing in inflammatory bowel disease—a true paradigm of success?" Gastroenterology & hepatology **8**(1), 29 (2012).

Biomedical Optics EXPRESS

6. J. Titus, E. Viennois, D. Merlin, and A. Unil Perera, "Minimally invasive screening for colitis using attenuated total internal reflectance fourier transform infrared spectroscopy," J. Biophotonics **10**(3), 465–472 (2017).
7. J. Titus, H. Ghimire, E. Viennois, D. Merlin, and A. Unil Perera, "Protein secondary structure analysis of dried blood serum using infrared spectroscopy to identify markers for colitis screening," J. Biophotonics **11**(3), e201700057 (2018).
8. H. Ghimire, P. Jayaweera, and A. U. Perera, "Longitudinal analysis of molecular alteration in serum samples of dextran sodium sulfate-induced colitis mice by using infrared spectroscopy," Infrared Phys. Technol. **97**, 33–37 (2019).
9. A. Tagore, W. Gonsalkorale, V. Pravica, A. Hajeer, R. McMahon, P. Whorwell, P. J. Sinnott, and I. V. Hutchinson, "Interleukin-10 (IL-10) genotypes in inflammatory bowel disease," Tissue Antigens **54**(4), 386–390 (1999).
10. W. E. Ip, N. Hoshi, D. S. Shouval, S. Snapper, and R. Medzhitov, "Anti-inflammatory effect of IL-10 mediated by metabolic reprogramming of macrophages," Science **356**(6337), 513–519 (2017).
11. E. Viennois, M. T. Baker, B. Xiao, L. Wang, H. Laroui, and D. Merlin, "Longitudinal study of circulating protein biomarkers in inflammatory bowel disease," J. Proteomics **112**, 166–179 (2015).
12. H. M. Van Dullemen, S. J. van Deventer, D. W. Hommes, H. A. Bijl, J. Jansen, G. N. Tytgat, and J. Woody, "Treatment of Crohn's disease with anti-tumor necrosis factor chimeric monoclonal antibody (cA2)," Gastroenterology **109**(1), 129–135 (1995).
13. A. Akazawa, I. Sakaida, S. Higaki, Y. Kubo, K. Uchida, and K. Okita, "Increased expression of tumor necrosis factor-α messenger RNA in the intestinal mucosa of inflammatory bowel disease, particularly in patients with disease in the inactive phase," J. Gastroenterol. **37**(5), 345–353 (2002).
14. K. Aden, A. Rehman, S. Waschina, W.-H. Pan, A. Walker, M. Lucio, A. M. Munez, R. Bharti, J. Zimmerman, J. Bethge, B. Schulte, B. Schulte, A. Franke, S. Nikolaus, J. O. Shroeder, D. Vandeputte, J. Raes, S. Szymczak, and P. Rosenstiel, "Metabolic functions of gut microbes associate with efficacy of tumor necrosis factor antagonists in patients with inflammatory bowel diseases," Gastroenterology **157**(5), 1279–1292.e11 (2019).
15. L. Peyrin-Biroulet, "Anti-TNF therapy in inflammatory bowel diseases: a huge review," Minerva gastroenterologica e dietologica **56**(2), 233–243 (2010).
16. R. Kühn, J. Löhler, D. Rennick, K. Rajewsky, and W. Müller, "Interleukin-10-deficient mice develop chronic enterocolitis," Cell **75**(2), 263–274 (1993).
17. P. J. Koelink, F. M. Bloemendaal, B. Li, L. Westera, E. W. Vogels, M. van Roest, A. K. Gloudemans, A. V. vant Wout, H. Korf, S. Vermeiere, A. A. te Velde, C. Y. Ponsioen, G. R. D Haens, J. S. Verbeek, T. L. Geiger, M. E. Wildenberg, and G. R. van den Brink, "Anti-TNF therapy in IBD exerts its therapeutic effect through macrophage IL-10 signalling," Gut **69**(6), 1053–1063 (2020).
18. T. Scheinin, D. M. Butler, F. Salway, B. Scallon, and M. Feldmann, "Validation of the interleukin-10 knockout mouse model of colitis: antitumour necrosis factor-antibodies suppress the progression of colitis," Clin. Exp. Immunol. **133**(1), 38–43 (2003).
19. S. Rakoff-Nahoum, L. Hao, and R. Medzhitov, "Role of toll-like receptors in spontaneous commensal-dependent colitis," Immunity **25**(2), 319–329 (2006).
20. J. Pedersen, M. Coskun, C. Soendergaard, M. Salem, and O. H. Nielsen, "Inflammatory pathways of importance for management of inflammatory bowel disease," World J. Gastroentero. **20**(1), 64 (2014).
21. L. Hancock and N. Mortensen, "How often do IBD patients require resection of their intestine?" Inflammatory Bowel Dis. **14**(suppl_2), S68–S69 (2008).
22. G. Bouguen and L. Peyrin-Biroulet, "*Surgery for adult Crohn's disease: what is the actual risk?*" ed: BMJ Publishing Group, 1178–1181 (2011).
23. E. Viennois, Y. Zhao, M. K. Han, B. Xiao, M. Zhang, M. Prasad, L. Wang, and D. Merlin, "Serum miRNA signature diagnoses and discriminates murine colitis subtypes and predicts ulcerative colitis in humans," Sci. Rep. **7**(1), 2520 (2017).
24. D. A. Naylor and M. K. Tahic, "Apodizing functions for Fourier transform spectroscopy," J. Opt. Soc. Am. A **24**(11), 3644–3648 (2007).
25. K. A. Chan and S. G. Kazarian, "Attenuated total reflection Fourier-transform infrared (ATR-FTIR) imaging of tissues and live cells," Chem. Soc. Rev. **45**(7), 1850–1864 (2016).
26. M. J. Baker, J. Trevisan, P. Bassan, R. Bhargava, H. J. Butler, K. M. Dorling, P. R. Fielden, S. W. Fogarty, N. J. Fullwood, K. A. Heys, C. Hughes, P. Lasch, P. L. Martin-Hirsch, B. Obinaju, G. D. Sockalingum, J. Sulé-Suso, R. J. Strong, M. J. Walsh, B. R. Wood, P. Gardner, and F. L. Martin, "Using Fourier transform IR spectroscopy to analyze biological materials," Nat. Protoc. **9**(8), 1771–1791 (2014).
27. S. G. Kazarian and K. A. Chan, "ATR-FTIR spectroscopic imaging: recent advances and applications to biological systems," Analyst **138**(7), 1940–1951 (2013).
28. A. W. Snyder and J. D. Love, "Goos-Hänchen shift," Appl. Opt. **15**(1), 236–238 (1976).
29. G. Clemens, J. R. Hands, K. M. Dorling, and M. J. Baker, "Vibrational spectroscopic methods for cytology and cellular research," Analyst **139**(18), 4411–4444 (2014).
30. S. G. Kazarian and K. A. Chan, "Micro-and macro-attenuated total reflection Fourier transform infrared spectroscopic imaging," Appl. Spectrosc. **64**(5), 135A–152A (2010).
31. W. Maddams and W. J. Mead, "The measurement of derivative ir spectra—I. Background studies," 38(4), 437–444 (1982).

Biomedical Optics EXPRESS

32. J. Grdadolnik, "ATR-FTIR spectroscopy: Its advantage and limitations," Acta Chimica Slovenica **49**(3), 631–642 (2002).
33. Å. Rinnan, F. van den Berg, and S. B. Engelsen, "Review of the most common pre-processing techniques for near-infrared spectra," TrAC, Trends Anal. Chem. **28**(10), 1201–1222 (2009).
34. P. D. Lewis, K. E. Lewis, R. Ghosal, S. Bayliss, A. J. Lloyd, J. Wills, R. Godfrey, P. Kloer, and L. A. Mur, "Evaluation of FTIR spectroscopy as a diagnostic tool for lung cancer using sputum," BMC Cancer **10**(1), 640 (2010).
35. Ø. Hammer, D. A. Harper, and P. D. Ryan, "PAST: Paleontological statistics software package for education and data analysis," Palaeontologia electronica **4**(1), 9 (2001).
36. R. Pribic, I. Vanstokkum, D. Chapman, P. I. Haris, and M. Bloemendal, "Protein secondary structure from Fourier transform infrared and/or circular dichroism spectra," Anal. Biochem. **214**(2), 366–378 (1993).
37. M. J. Baker, E. Gazi, M. D. Brown, J. H. Shanks, P. Gardner, and N. W. Clarke, "FTIR-based spectroscopic analysis in the identification of clinically aggressive prostate cancer," Br. J. Cancer **99**(11), 1859–1866 (2008).
38. L.-P. i. Choo, D. L. Wetzel, W. C. Halliday, M. Jackson, S. M. LeVine, and H. H. Mantsch, "In situ characterization of beta-amyloid in Alzheimer's diseased tissue by synchrotron Fourier transform infrared microspectroscopy," Biophys. J. **71**(4), 1672–1679 (1996).
39. M. Szczerbowska-Boruchowska, P. Dumas, M. Z. Kastyak, J. Chwiej, M. Lankosz, D. Adamek, and A. Krygowska-Wajs, "Biomolecular investigation of human substantia nigra in Parkinson's disease by synchrotron radiation Fourier transform infrared microspectroscopy," Arch. Biochem. Biophys. **459**(2), 241–248 (2007).
40. P. I. Haris, "Probing protein–protein interaction in biomembranes using Fourier transform infrared spectroscopy," Biochim. Biophys. Acta, Biomembr. **1828**(10), 2265–2271 (2013).
41. J. Kong and S. Yu, "Fourier transform infrared spectroscopic analysis of protein secondary structures," Acta Biochim. Biophys. Sin. **39**(8), 549–559 (2007).
42. J. J. Moré, "The Levenberg-Marquardt algorithm: implementation and theory," in *Numerical Analysis* 105–116 (Springer, 1978).
43. H. Ghimire, M. Venkataramani, Z. Bian, Y. Liu, and A. U. Perera, "ATR-FTIR spectral discrimination between normal and tumorous mouse models of lymphoma and melanoma from serum samples," Sci. Rep. **7**(1), 1–9 (2017).
44. H. Ghimire, C. Garlapati, E. A. Janssen, U. Krishnamurti, G. Qin, R. Aneja, and A. G. Unil Perera, "Protein Conformational Changes in Breast Cancer Sera Using Infrared Spectroscopic Analysis," Cancers **12**(7), 1708 (2020).
45. J. T. Pelton and L. R. McLean, "Spectroscopic Methods for Analysis of Protein Secondary Structure," Anal. Biochem. **277**(2), 167–176 (2000).
46. J. A. Pierce, R. S. Jackson, K. W. Van Every, P. R. Griffiths, and H. Gao, "Combined deconvolution and curve fitting for quantitative analysis of unresolved spectral bands," Anal. Chem. **62**(5), 477–484 (1990).
47. R. Sahu, S. Argov, A. Salman, M. Huleihel, N. Grossman, Z. Hammody, J. Kapelushnik, and S. Mordechai, "Characteristic absorbance of nucleic acids in the Mid-IR region as possible common biomarkers for diagnosis of malignancy," Technol. Cancer Res. Treat. **3**(6), 629–638 (2004).
48. J. B. Reitsma, A. S. Glas, A. W. Rutjes, R. J. Scholten, P. M. Bossuyt, and A. H. Zwinderman, "Bivariate analysis of sensitivity and specificity produces informative summary measures in diagnostic reviews," J. Chronic Dis. **58**(10), 982–990 (2005).
49. A.-M. Šimundić, "Measures of diagnostic accuracy: basic definitions," EJIFCC **19**(4), 203 (2009).
50. P. G. Andrus and R. D. Strickland, "Cancer grading by Fourier transform infrared spectroscopy," Biospectroscopy **4**(1), 37–46 (1998).
51. C. Petibois, V. Rigalleau, A.-M. Melin, A. Perromat, G. Cazorla, H. Gin, and H. Deleris, "Determination of glucose in dried serum samples by Fourier-transform infrared spectroscopy," Clin. Chem. **45**(9), 1530–1535 (1999).
52. A. Yamanaka, A. Hashimoto, T. Matsuo, M. Kanou, K.-I. Suehara, and T. Kameoka, "Analysis of kinetic uptake phenomena of monosaccharide and disaccharide by suspension TBY-2 cells using an FT-IR/ATR method," Bioprocess Biosyst. Eng. **30**(6), 457–468 (2007).
53. Z. Movasaghi, S. Rehman, and D. I. ur Rehman, "Fourier transform infrared (FTIR) spectroscopy of biological tissues," Appl. Spectrosc. Rev. **43**(2), 134–179 (2008).
54. B. R. Wood, M. A. Quinn, F. R. Burden, and D. McNaughton, "An investigation into FTIR spectroscopy as a biodiagnostic tool for cervical cancer," Biospectroscopy **2**(3), 143–153 (1998).
55. G. I. Dovbeshko, N. Y. Gridina, E. B. Kruglova, and O. P. Pashchuk, "FTIR spectroscopy studies of nucleic acid damage," Talanta **53**(1), 233–246 (2000).
56. P. Ramalingam, Y. P. Reddy, K. V. Kumar, B. R. Chandu, and K. Rajendran, "Evaluation of metformin hydrochloride in Wistar rats by FTIR-ATR spectroscopy: A convenient tool in the clinical study of diabetes," J. Nat. Sc. Biol. Med. **5**(2), 288 (2014).
57. H. Fabian, M. Jackson, L. Murphy, P. H. Watson, I. Fichtner, and H. H. Mantsch, "A comparative infrared spectroscopic study of human breast tumors and breast tumor cell xenografts," Biospectroscopy **1**(1), 37–45 (1995).
58. H. Yang, S. Yang, J. Kong, A. Dong, and S. Yu, "Obtaining information about protein secondary structures in aqueous solution using Fourier transform IR spectroscopy," Nat. Protoc. **10**(3), 382–396 (2015).
59. A. Tesija Kuna, "Serological markers of inflammatory bowel disease," Biochem. Med. **23**(1), 28–42 (2013).
60. J. Barahona-Garrido, H. Sarti, M. Barahona-Garrido, J. Hernández-Calleros, E. Coss-Adame, and S. Garcia-Saenz, *et al.*, "Serological markers in inflammatory bowel disease: a review of their clinical utility," Revista de gastroenterologia de Mexico **74**(3), 230–237 (2009).
61. E. A. Scoville, M. M. Allaman, C. T. Brown, A. K. Motley, S. N. Horst, C. S. Williams, T. Koyama, Z Zhao, D. Beaulieu, K. T. Wilson, and L. A. Coburn, "Alterations in lipid, amino acid, and energy metabolism distinguish

Biomedical Optics EXPRESS

Crohn's disease from ulcerative colitis and control subjects by serum metabolomic profiling," Metabolomics **14**(1), 17 (2018).

62. D. M. Wiese, S. N. Horst, C. T. Brown, M. M. Allaman, M. E. Hodges, J. C. Slaughter, J. P. Druce, D. B. Beaulieu, D. A. Schwartz, K. T. Wilson, and L. A. Coburn, "Serum fatty acids are correlated with inflammatory cytokines in ulcerative colitis," PLoS One **11**(5), e0156387 (2016).
63. D. K. Rex, J. C. Lappas, D. D. Maglinte, M. C. Malczewski, K. A. Kopecky, and E. M. Cockerill, "Enteroclysis in the evaluation of suspected small intestinal bleeding," Gastroenterology **97**(1), 58–60 (1989).